THE EMBO JOURNAL

microRNA-17-92 cluster is a direct Nanog target and controls neural stem cell through Trp53inp1

Neha Garg[1], Agnese Po[1], Evelina Miele[1,2],
Antonio Francesco Campese[1],
Federica Begalli[1], Marianna Silvano[1],
Paola Infante[1,2], Carlo Capalbo[1],
Enrico De Smaele[3], Gianluca Canettieri[1],
Lucia Di Marcotullio[1], Isabella Screpanti[1,2],
Elisabetta Ferretti[3],* and
Alberto Gulino[1,4],*

[1]Department of Molecular Medicine, University of Rome 'La Sapienza', Rome, Italy, [2]Center for Life Nano Science@Sapienza, Istituto Italiano di Tecnologia, Rome, Italy, [3]Department of Experimental Medicine, University of Rome 'La Sapienza', Rome, Italy and [4]Neuromed Institute, Pozzilli, Italy

The transcription factor Nanog plays a critical role in the self-renewal of embryonic stem cells as well as in neural stem cells (NSCs). microRNAs (miRNAs) are also involved in stemness regulation. However, the miRNA network downstream of Nanog is still poorly understood. High-throughput screening of miRNA expression profiles in response to modulated levels of Nanog in postnatal NSCs identifies miR-17-92 cluster as a direct target of Nanog. Nanog controls miR-17-92 cluster by binding to the upstream regulatory region and maintaining high levels of transcription in NSCs, whereas Nanog/promoter association and cluster miRNAs expression are lost alongside differentiation. The two miR-17 family members of miR-17-92 cluster, namely miR-17 and miR-20a, target Trp53inp1, a downstream component of p53 pathway. To support a functional role, the presence of miR-17/20a or the loss of Trp53inp1 is required for the Nanog-induced enhancement of self-renewal of NSCs. We unveil an arm of the Nanog/p53 pathway, which regulates stemness in postnatal NSCs, wherein Nanog counteracts p53 signals through miR-17/20a-mediated repression of Trp53inp1.

Introduction

Nanog encodes a homeobox transcription factor expressed in the inner cells of blastocyst (ICM), as well as in the embryonic stem (ES) and in germline cells (Chambers *et al*, 2003;

*Corresponding authors. A Gulino, Department of Molecular Medicine, Sapienza University, Viale Regina Elena, 291-00161 Rome, Italy. Tel.: +39 064464021; Fax: +39 0649255660; E-mail: alberto.gulino@uniroma1.it or E Ferretti, Department of Experimental Medicine, Sapienza University, Viale Regina Elena, 291-00161 Rome, Italy. Tel.: +39 0649255135; Fax: +39 0649255660; E-mail: elisabetta.ferretti@uniroma1.it

Mitsui *et al*, 2003). Nanog has been reported to belong to a 'core program' of so-called 'stemness genes', also conferring cytokine-independent (e.g., LIF, BMP, and GDF) self-renewal to ES cells (Mitsui *et al*, 2003). As a part of such a program, Nanog transcription is modulated by a variety of transcription factors involved in stemness (e.g. FoxD3, Oct4/Sox2, Zfp143, TCF3, p53 and the Hedgehog (Hh) pathway effector Gli1), which bind to its proximal promoter region (Pan and Thomson, 2007; Chen *et al*, 2008a, b; Po *et al*, 2010). Indeed, reprogramming of differentiated somatic cells to induced pluripotent stem cells (iPSCs) by Oct4, Sox2, c-Myc, and Klf4, reactivates the expression of Nanog (Takahashi and Yamanaka, 2006; Brambrink *et al*, 2008); in addition, Nanog overexpression itself cooperates with some of the above stemness factors (i.e., c-myc) in cell reprogramming (Lewitzky and Yamanaka, 2007), indicating that Nanog has an important function in determining stemness. To this regard, Nanog is required to drive the cell transit to ground-state pluripotency in both ES cells and iPSC (Silva *et al*, 2009).

A role for Nanog has also recently been described in postnatal cerebellar neural stem cells (NSCs), where Hh/Gli-dependent Nanog overexpression sustains self-renewal (Po *et al*, 2010; Zbinden *et al*, 2010). In spite of our good understanding of the mechanisms regulating the expression of these stemness drivers, there is incomplete knowledge of their target genes and of how the resulting regulatory network operates in order to determine stem cell features. MicroRNAs (miRNAs) have emerged as important players in the control of stem cell behaviour (Blakaj and Lin, 2008). MiRNAs bind to the 3′untranslated region (3′UTR) of target mRNAs to repress their translation and stability (Stefani and Slack, 2008). Previous reports have described miRNAs (i.e., miR-302-367, miR-134, and miR-296) targeting Nanog in ES cells (Tay *et al*, 2008a, b); however, whether Nanog regulates the miRNA network in stem cell context has not been elucidated yet.

To this end, we analysed high-throughput miRNA profiling in NSCs upon modulation of Nanog expression. This study allowed us to identify specific miRNAs controlled by Nanog, including miR-17-92 cluster. The two miR-17 family members of miR-17-92 cluster, namely miR-17 and miR-20a, negatively control p53-induced nuclear protein 1 (Trp53inp1), a downstream component of p53 pathway. In NSCs, Nanog enhances miR-17 family and inhibits the expression of Trp53inp1, thus promoting self-renewal. Our findings show that Nanog controls stem cells through miR-17/20a-mediated repression of Trp53inp1, thus blunting the known opposing activity of p53 upon Nanog, in order to maintain NSC. Therefore, we identified a previously unsuspected backward arm of the Nanog/p53 pathway cross-regulation of stemness.

Results

High-throughput miRNA profiling in high- and low-Nanog expressing cells

To identify miRNA regulated by Nanog, we have chosen different cell models in which to modulate the levels of

Nanog expression: high-Nanog and low-Nanog expressing cells. Indeed, we have previously described that Prominin-1^{+} cells, reported to populate the postnatal mouse cerebellum (Lee et al, 2005), are characterized by high Nanog levels and are able to form neurospheres (Po et al, 2010).

To select this 'high Nanog NSC' (HN-NSC) cell population, we infected neurospheres with lentiviral vector expressing GFP under the control of Nanog promoter (Nanog/GFP) or a control CMV promoter (CMV/GFP) and sorted the GFP-positive cells. Nanog/GFP-positive cells presented, as expected, higher levels of Nanog and stemness-related markers, Gli1 and prominin-1, compared to the CMV/GFP (Figure 1A; Supplementary Figure S1A). We also generated an additional model of high-Nanog expressing cells by transfecting a Nanog-encoding vector (or of an empty vector as a control) in neurospheres (Figure 1B; Supplementary Figure S1B).

Conversely, downregulation of Nanog or low-Nanog expressing cells (LN-NSCs) were obtained culturing HN-NSC under differentiation conditions (Figure 1C; Supplementary Figures S1C and S1D). Either platelet derived growth factor (PDGF) or retinoic acid (RA) prevented neurosphere formation from dispersed secondary neurospheres and resulted in cells with a differentiated morphology (Supplementary Figure 1C) and expressing markers of differentiation. Differentiated NSCs presented higher levels of the neuronal differentiation marker βIII-tubulin, while the stemness determinant Nanog and the Hh pathway components Smo and Gli1 were reduced (Figure 1C; Supplementary Figure S1D).

In addition, LN-NSCs have been also obtained by siRNA-mediated targeting of Nanog (siNanog; Figure 1D and Supplementary Figure S1E). Clonogenic assays of Nanog-depleted NSCs revealed a lower capacity to form neuro-
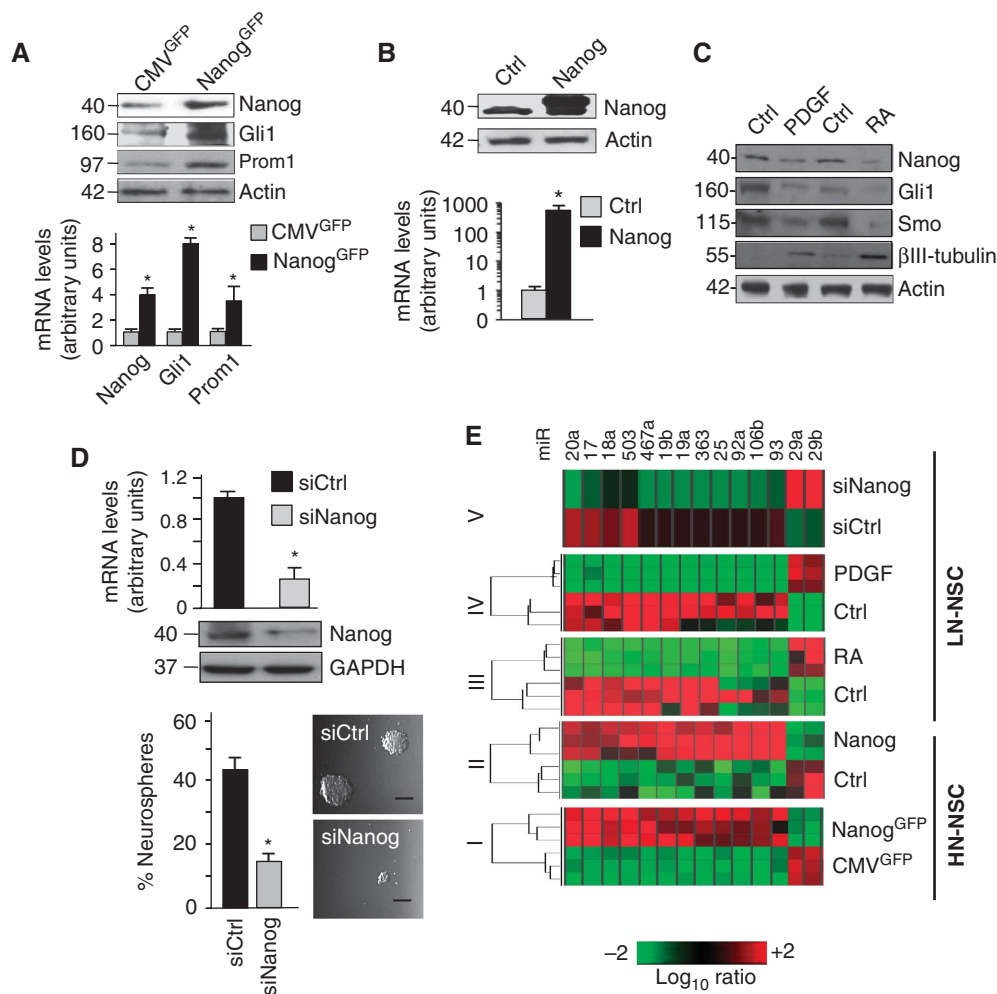

Figure 1 Features of neurospheres with respect to Nanog expression. (**A**) Western blot and mRNA levels of Nanog, Gli1, and Prominin-1 (Prom1) in GFP-sorted cells infected with Nanog-GFP or CMV-GFP control lentiviral vector. Graph error bars indicate s.d. calculated on at least three independent experiments. *$P < 0.05$ versus CMV-GFP. Densitometry of western blot is in Supplementary Figure S1A. (**B**) Western blot for protein and mRNA levels of Nanog after overexpression of Nanog or Empty (Ctrl) vectors. Bars represent the mean of three independent experiments ± s.d. *$P < 0.05$ versus Ctrl. (see Supplementary Figure S1B for densitometry). (**C**) Representative image of protein levels of stemness (Nanog), Hh (Gli1 and Smo), and differentiation (βIII-tubulin) markers in HN-NSC treated with PDGF or RA (4 days) (see Supplementary Figure S1D for densitometry). (**D**) SiRNA-mediated silencing of Nanog (siNanog): in the upper part, mRNA levels and western blot of Nanog; in the lower part, bright-field images of secondary neurosphere-forming assay of NSCs after Nanog silencing (scale bar, 100 mm) and the relative percentage of neurosphere-forming capability. Bars represent the mean of three independent experiments ± s.d. *$P < 0.05$ versus siCtrl. (**E**) Hierarchical clustering of differentially expressed miRNA, in high (HN-NSC: Nanog-GFP, Nanog overexpressing cells (Nanog) or low Nanog cells (LN-NSC: 4-day RA or PDGF treated; silencing of Nanog (siNanog). All data are normalized against the relative controls. A green-red colour scale depicts normalized miRNA expression levels (green, low; red, high). Source data for this figure is available on the online supplementary information page.

spheres (Figure 1D, bottom ; Supplementary Figure S1F). All of the above cell models were therefore classified as 'low Nanog' NSCs (LN-NSC). We performed high-throughput miRNA expression profiling on all HN-NSC and LN-NSC models. In the HN-NSC contexts, we found a total of 69 differentially expressed miRNAs (54 upregulated and 15 downregulated, with respect to relative controls) (Supplementary Figure S2; Supplementary Table S1). In the LN-NSC models, a total of 105 miRNAs were differentially expressed (84 downregulated and 21 upregulated, compared to relative controls) (Supplementary Figure S2; Supplementary Table S2). Cross-comparison of all clustered miRNAs allowed us to generate a 'consensus' of 12 miRNAs, which are upregulated in all models of HN-NSC and down-regulated in all models of LN-NSC, and 2 miRNAs which behave in the opposite way (Figure 1E; Supplementary Tables S1 and S2). These miRNAs are more likely to be directly regulated by Nanog expression. Interestingly, our screening approach unveiled Nanog modulation of the two paralogous polycistronic miRNA clusters miR-17-92 and miR-106b-25 (Figure 1E; Supplementary Tables S1 and S2) previously reported to modulate various cell-cycle regulators, potentially involved in stem/progenitor cell control (Li et al, 2011; Vidigal and Ventura, 2012).

Indeed, it has been described that miR-17-92 cluster enhances the proliferation of cerebellar granule cell progenitors (GCPs) (Northcott et al, 2009; Uziel et al, 2009), while an miR-106b-25 cluster has been reported to regulate adult NSC proliferation and neuronal differentiation (Brett et al, 2011). Since GCPs originate during the differentiation of NSCs both in vitro and in vivo (Klein et al, 2005; Po et al, 2010), we focused our further study on these clusters.

MiR-17-92 cluster is a direct Nanog target in NSC

We first validated profiling data by single assay QPCR (Figure 2A). To verify a direct transcriptional Nanog control on the two miRNA clusters, miR-17-92 and miR-106b-25, their genomic cis-regulatory regions were investigated. To this end, we looked for the presence of putative Nanog responsive elements (NREs) using the Genomatix Mathinspector software package, by scanning 1.5 kb of mouse genomic sequence located upstream of the predicted miR-17-92 cluster transcription start site (TSS) and the sequences upstream miR-106b-25 cluster TSS together with the promoter of the Mcm7 gene hosting this cluster (Kim and Kim, 2007). We identified s1 (−241 bp), s2 (−874 bp), and s3 (−1063 bp) sites in miR-17-92 locus (Figure 2B; Supplementary Figure S3) as well as s1–s3 (−45 bp, −480 bp, and −1403 bp, respectively) and s4 (−356 bp of Mcm7 promoter) in miR-106b-25 cluster as putative NRE (Supplementary Figure S4A). Next, we examined the in vivo occupancy of endogenous Nanog on these putative cis-regulatory sequences in HN-NSCs. Chromatin immunoprecipitation (ChIP) experiments revealed that Nanog was recruited on the s1, s2, and s3 sites in miR-17-92 cluster (Figure 2C). Nanog recruitment was accompanied by acetylation of histone H3 in the same promoter sequence, as a marker of a transcriptionally active region. After RA treatment of HN-NSC, Nanog levels were reduced together with abrogation of its binding on NREs (Figure 1C) and a decrease in acetylated histone H3 (Figure 2C). In contrast, s1–s4 sites of miR-106b-25 cluster did not recruit Nanog, suggesting that this cluster is not subjected to a direct transcriptional regulation by

Nanog (Supplementary Figure S4B). To confirm the role of Nanog in the control of miR-17-92 cluster transcription, we generated and tested constructs in which the wild-type or mutated miR-17-92 upstream regulatory region was driving luciferase reporter. We found that either overexpression or siNanog significantly enhanced or inhibited, respectively, miR-17-92 promoter activity (Figure 2D). Accordingly, enhanced miR-17-92 promoter-driven luciferase activity was observed in Nanog promoter-GFP-sorted cells, compared to controls, proving that Nanog-dependent miR-17-92 transcription is enriched in Nanog$^+$ cells (Figure 2D). We also generated mutant reporters (Δs1, Δs2, and Δs3) that have altered sequences in the Nanog-binding sites, which prevented Nanog-induced luciferase activity, suggesting that the presence of these NREs is required to activate transcription of miR-17-92 cluster (Figure 2D). As a positive control, the transcriptional activity of Nanog on its own promoter was tested, as described earlier (Wu et al, 2006). Overall, these findings demonstrated that miR-17-92 cluster is a direct transcriptional target of Nanog.

MiR-17-20a targets Trp53inp1 in NSC

To better understand the network of Nanog/miR-17-92 in NSCs, we searched for potential targets of this cluster. Mir-17-92 cluster consists of six miRNAs that are processed from a common precursor transcript and that can be subgrouped into four families based on their 'seed' sequence, including miR-17 family (miR-17 and miR-20a), miR-18 family (miR-18a), miR-19 family (miR-19a and miR-19b), and miR-92 family (miR-92a). We searched for putative targets of each family using the prediction algorithms of PicTar, TargetScan, and MiRBase. We found that, among miR-17-92 cluster putative gene targets, the most highly downregulated or upregulated gene in Nanog-GFP and in siNanog cells, respectively, was Trp53inp1 (Supplementary Figures S5A and B). Trp53inp1 is an anti-proliferative protein within the p53 pathway, being transcriptionally activated by p53 and enhancing its activity upon its responsive genes, that is, p21 (Okamura et al, 2001; Tomasini et al, 2001, 2002). The other miR-17-92 putative target genes evaluated resulted just slightly (i.e., p21 and Rb1) or not regulated (Supplementary Figures S5A and B). Since Trp53inp1 was the most consistently gene regulated by Nanog in NSCs (Supplementary Figures S5A and B) and in the light that p53 pathway is a master stemness regulator (Meletis et al, 2006), we focussed on the characterization of Trp53inp1 by Nanog/miR-17/92 axis. By base-pairing complementation, we found that the 3′UTR of Trp53inp1 encompasses two putative binding regions (1016–1021 nt and 4268–4275 nt) bearing significant complementarities against both miR-17 and miR-20a (Figure 3A; Supplementary Figure S6A). Abrogation of miR-17 family members, through LNA-modified antagomirs (LNA), confirmed the Nanog-dependent up-regulation of Trp53inp1, while other genes evaluated resulted unaffected (Supplementary Figure S6B).

The two 3′UTR elements of Trp53inp1 and the sequences of their miR-17 family putative binding sites are extremely conserved among different species (mouse, rat, monkey, and human orthologues) (not shown), suggesting a functional role. Therefore, to investigate whether Trp53inp1 is a 'bona fide' target of miR-17 family members, a mouse Trp53inp1 4418 bp 3′UTR fragment was divided into two
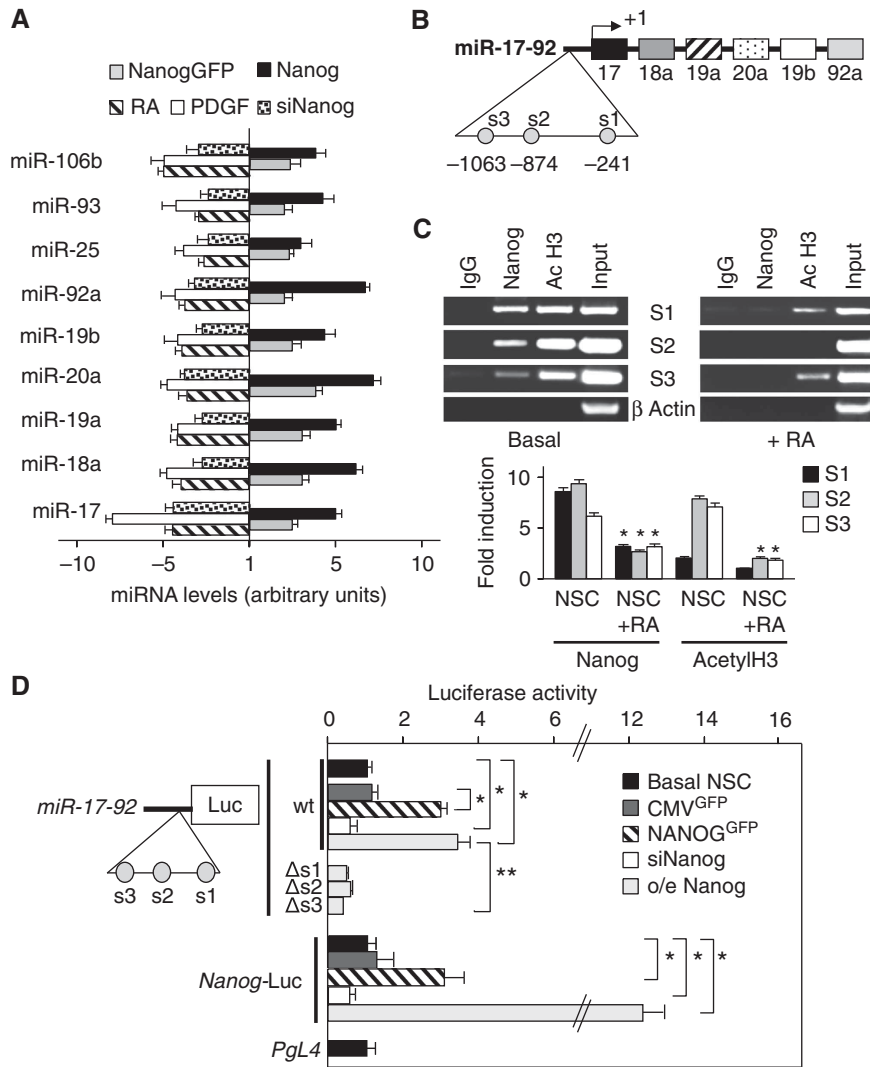
Figure 2 Nanog transcriptionally controls miR-17-92 cluster expression. (**A**) RT–qPCR analysis of individual microRNA miR-17-92 and miR-106b-25 clusters in HN-NSC (Nanog-GFP and Nanog overexpressing cells) or LN-NSC (NSC after RA and PDGF treatment and Nanog silencing). Bars represent the mean of three independent experiments ± s.d. $P < 0.05$ versus respective control for all. (**B**) Representation of microRNA-17-92 cluster upstream regulatory region showing the putative Nanog responsive elements (NREs), labelled as s1, s2, and s3 (depending upon the distance from TSS, s1 closest and s3 farthest). (**C**) ChIP (upper panel) and qPCR-ChIP (lower panel) assays from untreated or RA-treated NSC using anti-Nanog or anti-acetyl-H3 antibodies. Eluted DNA was PCR amplified for s1, s2, and s3 NRE of miR-17-92 cluster upstream region or β-actin with primers shown in Materials and methods. Real-time qPCR-ChIP results are expressed as fold induction versus β-actin-amplified ChIP controls. Bars represent the mean of three independent experiments ± s.d. *$P < 0.05$ versus untreated cells. (**D**) Relative luciferase activity driven by mouse miR-17-92 cluster wild-type (wt) upstream regulatory region (-1107 bp, as reported in Supplementary Figure S3) in basal condition, in Nanog-GFP versus CMV-GFP cells and after silencing and overexpression of Nanog. Mutants (Δs1, Δs2, and Δs3) of Nanog-binding sites are shown in the presence of Nanog overexpression in NSC. As a control, luciferase activity of mouse Nanog promoter (-2500 bp) reporter construct carrying Nanog consensus sequence (*Nanog*-Luc) in all contexts analysed is shown. Luciferase activity of PgL4 (empty vector) reporter construct (as a mock control) is also reported. Results are normalized with pRL-CMV-Renilla Luciferase. Bars represent the mean of at least three independent experiments performed in triplicate ± s.d. *$P < 0.01$. **$P < 0.005$. Source data for this figure is available on the online supplementary information page.

clones comprising 1–2275 bp (site 1) and 2131–4418 bp (site 2) regions harbouring the putative miRNA-binding sites and cloned downstream the luciferase reporter gene (Supplementary Figure S7A). Luciferase activity of Trp53inp1 3′UTR-site 1 was markedly reduced by 40 and 50% in cells transfected respectively with miR-17 or miR-20a, while these miRNAs decreased 3′UTR site 2 activity by 45 and 55%, respectively (Figure 3B). Conversely, site 1 or site 2 deletion from Trp53inp1 3′UTR abrogated miR-17 or miR-20a-reduced luciferase activity as compared to their wild-type 3′UTR, suggesting that these sites are required for miRNA binding and activity (Figure 3B). Remarkably,

Trp53inp1-3′UTR-Luciferase activity was reduced in Nanog[GFP] NSCs or increased after siNanog, suggesting a relevance of this regulation in high or low Nanog contexts (Figure 3C). Accordingly, inactivation of each miRNA by specific LNA anti-miR induced an increase in Trp53inp1 mRNA and protein levels (Figure 3D; Supplementary Figure S7B). Overall, these findings demonstrated that Trp53inp1 is a direct target of the Nanog/miR-17 family axis.

In order to verify the presence of Nanog/miR-17/20a/Trp53inp1 axis *in vivo*, we derived Prominin-1[+] NSC from fresh mouse cerebella, as previously described (Po *et al*, 2010). Prominin-1[+] FACS-sorted cells displayed high levels
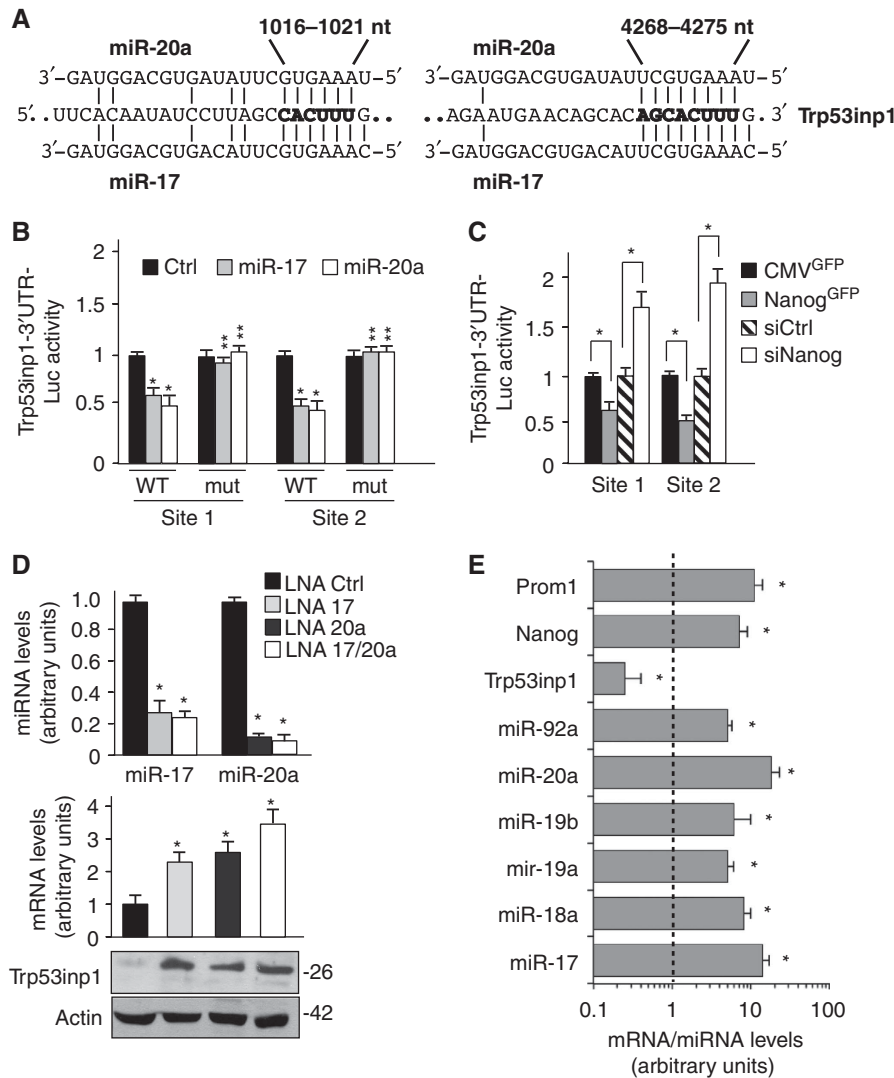
Figure 3 miR-17 family modulates Trp53inp1 expression. (**A**) Schematic representation of 3′UTR sequence from mouse Trp53inp1 indicating the putative miRNA-binding sites (shown in bold) and their nucleotide (nt) position on the sequence. Other details are reported in Supplementary Figure S6A. (**B**) Luciferase activity of Trp53inp1 wild-type 3′UTR vectors (wt) or its mutant derivative lacking the miRNA-binding sites (mut) in NSC overexpressing the indicated miRNA. Results are normalized with pRL-CMV-Renilla Luciferase control (Ctrl). Graph error bars indicate s.d. calculated on at least three independent experiments. *$P<0.05$ versus Ctrl and **$P<0.05$ versus corresponding wt-UTR. (**C**) Luciferase activity of Trp53inp1 wild-type 3′UTR vectors in Nanog-GFP or CMV-GFP sorted NSC and after siNanog or sicontrol (Ctrl). Bars represent the mean of three independent experiments ± s.d. *$P<0.05$ versus relative control. (**D**) LNA mediated knockdown of miR-17/20a. Upper panel shows miRNA levels after specific knockdown or LNA control (LNA ctrl); in lower part, mRNA level and western blot are shown. Graph error bars indicate s.d. calculated on at least three independent experiments. *$P<0.05$ versus LNA ctrl. Relative densitometry of western blot is reported in Supplementary Figure S7B. (**E**) Gene expression analysis of Prom1, Nanog, and Trp53inp1 mRNA and microRNA from miR-17-92 cluster of FACS-sorted Prominin1[+] (Prom1^{+}) versus Prominin1[−] (Prom1^{−}) cells. Results were obtained from the cell pools derived from eight fresh mouse cerebella of 4-day-old mice. Bars represent the mean of three independent experiments ± s.d. *$P<0.05$ versus Prom1^{−} cells (dashed line). Source data for this figure is available on the online supplementary information page.

of both Nanog and miR-17-92 cluster, while Trp53inp1 expression was very low, compared to sorted Prominin-1^{−} cells (Figure 3E). These results show that, in analogy with neurospheres, in 'ex vivo' NSC, miRNA 17-92 cluster and Nanog are highly expressed, while Trp53inp1 is downregulated, thus supporting the presence of a Nanog/miR-17/20a/Trp53inp1 axis in a 'bona fide' NSC context.

Nanog/miR-17/20a/Trp53inp1 controls cell cycle and proliferation

It has been described a p53-induced negative regulation of both Nanog expression (Lin *et al*, 2005; Kawamura *et al*, 2009) and NSC self-renewal (Meletis *et al*, 2006), aimed at

restraining the overproliferation of NSCs by limiting the frequency of self-renewing divisions. The Nanog-dependent control of Trp53inp1, that we have described, would suggest a backward regulation of p53 pathway Nanog cross-talk, where Nanog counteracts the growth-limiting function of p53 pathway.

To verify this hypothesis, we first checked how Nanog/miR-17/20a/Trp53inp1 axis is regulated along the cell cycle. NSCs were synchronized through a 12-h treatment with nocodazole, resulting in G2-phase accumulation (Figure 4A). After nocodazole withdrawal, synchronized cells were monitored along cell-cycle phases (Figure 4B; Supplementary Figure S8) for Nanog and Trp53inp1 levels
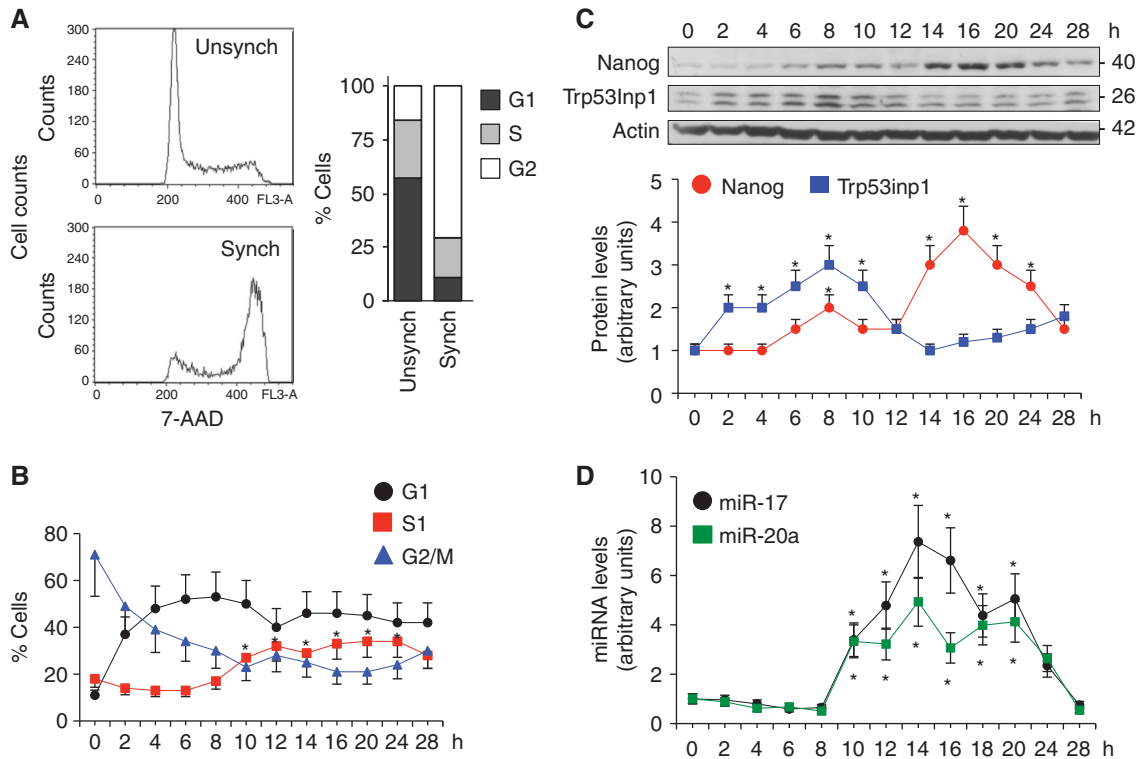
Figure 4 Nanog/miR-17/20a/Trp53inp1 axis in NSC cycle. (**A**) Left: representative images of flow cytometry show NSC, 7-AAD stained, cell-cycle profile before (Unsynch) and after Nocodazole synchronization (Synch); Right: graph showing the percentage of cells in given cell-cycle phases. Graph represents the mean of three independent experiments. (**B**) Line chart of flow cytometry cell cycle showing the percentage of NSC (% cells) in different cell-cycle phases after release from nocodazole treatment (0 h time) as obtained by 7-AAD staining. Percentages have been obtained at 0, 2, 4, 6, 8, 10, 12, 14, 16, 20, 24, and 28 h. Time points are expressed as mean ± s.d. from three independent experiments. *$P < 0.05$ versus T0 (nocodazole withdrawal). Representative flow cytometry images are shown in Supplementary Figure S9. (**C**) Western blot representative image (upper) and densitometry (bottom) of Nanog and Trp53inp1 after release from nocodazole synchronization. Results are expressed as mean ± s.d. from three independent experiments. *$P < 0.05$ versus T0. (**D**) Graph shows miR-17 and miR-20a levels after release from nocodazole synchronization. Results are expressed as mean ± s.d. from three independent experiments. *$P < 0.05$ versus T0. Source data for this figure is available on the online supplementary information page.

(Figure 4C). Nanog levels increased as early as 6–8 h after drug withdrawal (time 0 h), $P < 0.05$ versus T0 (Figure 4C), which marks cells moving from G1 to S phase (Figure 4B; Supplementary Figure S8). Such increase preceded the upregulation of miR-17/20a levels (between 8 and 10 h) ($P < 0.05$ versus T0), followed by a decrease in Trp53inp1 levels (between 10 and 12 h) ($P < 0.05$ versus T0) (Figures 4C and D). As cells moved along S phase after 8 h, Nanog and Trp53inp1 levels arose or declined, respectively (Figures 4B and C). Remarkably, this modulation was associated with increased miR-17/20a levels in early S phase, which would explain Trp53inp1 low levels (Figures 4C and D).

The above findings suggest that Nanog is functionally linked to cell proliferation rate, as supported by the ability of Nanog silencing to reduce BrdU uptake in HN-NSCs (Figure 5A; Supplementary Figure S9). Moreover, double staining with BrdU and 7-AAD allowed us to follow HN-NSC cell cycle after Nanog silencing, that resulted in a reduction in S phase together with an increase in G0/G1 (Figure 5B; Supplementary Figure S10). Accordingly, by labelling NSC using a fluorescent anti-Nanog antibody, we observed that the majority of Nanog⁺ cells were in the S phase (Figure 5C). A similar increase in Nanog⁺ cells was observed after the treatment with the Hh agonist SAG, previously shown to enhance NSC proliferation (Po et al, 2010) (Figure 5D).

Overall, these observations indicate that Nanog enhances the proliferation of NSCs by promoting G1/S transition, supporting the previously described findings in human ES cells, in which Nanog enhances S-phase entry (Zhang et al, 2009).

miR-17/20a is required for Nanog effects on NSC, through inactivation of Trp53inp1

To further investigate the mechanism of Nanog-dependent Trp53inp1 regulation, we first examined how Trp53inp1 levels changed upon Nanog modulation. We observed a reduced expression of Trp53inp1 in both Nanog^GFP and SAG-treated NSC (Figures 6A and B). Conversely, siNanog reverted Trp53inp1 expression levels (Figure 6C). To confirm that Nanog effect on Trp53inp1 is mediated by miR-17/20a, we inhibited these miRNAs with specific LNA antagomirs (LNA 17/20a) in the presence of Nanog overexpression. Nanog overexpression induced a decrease in Trp53inp1; however, in the presence of miR-17/20a silencing, Nanog did not inhibit Trp53inp1, thus proving that its action on Trp53inp1 is mediated by these two miRNAs (Figure 6D). Moreover, to directly address the role of Trp53inp1 and miR-17/20a in cell proliferation, we transfected HN-NSC with a combination of LNA anti-miR-17 and -20a. LNA antagomir increased Trp53inp1 protein levels (Figure 7A) and significantly reduced cell proliferation rates (Figure 7B;
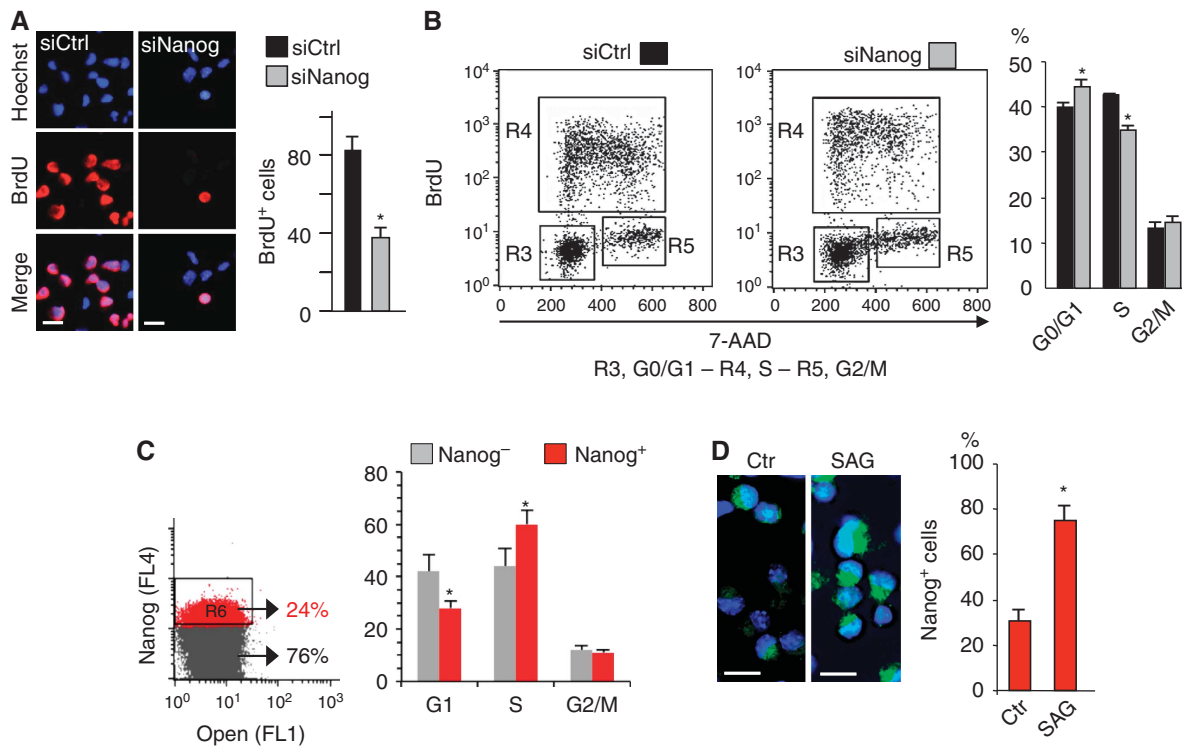
Figure 5 Nanog regulates NSC proliferation. (**A**) Immunofluorescence staining of BrdU uptake depicting Hoechst (blue) and BrdU (red) after transfection of NSC with control or siNanog (scale bar, 5 μm). Bars represent the mean of three independent experiments ± s.d. *$P < 0.05$ versus siCtrl. (**B**) Analysis of cell cycle of Nanog-depleted NSC. Left: FACS images show BrdU and 7-AAD profile after Nanog silencing or control (siCtrl); on the right, the histogram shows the percentage of cells in each cell-cycle phase. Graph error bars indicate s.d. calculated on at least three independent experiments. *$P < 0.05$ versus siCtrl. (**C**) Flow cytometry images showing Nanog-positive and -negative cells (left panel), and their percent distribution in cell-cycle phase (right panel) in NSC. The figure is representative of three independent experiments. *$P < 0.05$ versus Nanog-negative cells. (**D**) Immunofluorescence staining of Nanog (green) in NSCs untreated and treated with SAG (scale bar, 5 μm). *$P < 0.05$ versus control (Ctr) (mean values ± s.d. from three experiments).

Supplementary Figure S11). To confirm the anti-proliferating role of Trp53inp1 in this context, we prevented the LNA-miR17/20a-mediated upregulation of Trp53inp1 by specific Trp53inp1 silencing (siTrp53inp1) (Figure 7A). Trp53inp1 silencing rescued the reduced cell proliferation induced by LNA anti-miR alone (Figure 7B). These observations support that Trp53inp1 reduced NSC proliferation rate induced by loss of miR-17/20a. Since Nanog drives NSC proliferation, we then asked whether this effect was mediated by the decrease in Trp53inp1 through upregulation of miR-17/20a. As shown in Figure 7C, siNanog resulted in increased Trp53inp1 levels, an effect prevented by simultaneous overexpression of miR-17/20a or siTrp53inp1 (Figure 7C). Remarkably, the reduction of BrdU uptake in Nanog-depleted NSCs was also abrogated by miR-17/20a overexpression or by siTrp53inp1 (Figure 7C; Supplementary Figure S12). Finally, to better understand the effect of Nanog/miR17/20a/Trp53inp1 axis upon cell cycle, we carried out FACS analysis with BrdU and 7-AAD double staining, to monitor cell-cycle phases (Supplementary Figure S10). According to results shown above, a decrease in S phase BrdU$^+$ cells was observed in NSC after Nanog silencing, an effect reverted by Trp53inp1 knockdown or by miR-17/20a overexpression (Figure 7D). Consistently, cell-cycle analysis showed that LNA-miR-17/20a-induced reduction in S-phase cells was reverted by siTrp53inp1 and was not affected by Nanog overexpression (Figure 7E; Supplementary Figure S10). Collectively, these findings suggest that Nanog, miR-17/20a, and Trp53inp1 are involved in the control of

NSC proliferation and S-phase entry through Nanog-induced upregulation of miR-17/20a and consequent downregulation of p53 pathway component Trp53inp1.

Nanog-miR-17/20a-Trp53inp1 axis controls NSC self-renewal

A critical property of stem cells is self-renewal, summarized by the ability to form neurospheres derived from the clonal expansion of individual stem cells, when cultured *in vitro*. We have previously reported that this property is driven by Nanog in NSCs (Po *et al*, 2010). To elucidate the functional role of miR-17/20a in NSCs self-renewal, we overexpressed these two LNA anti-miR, alone or in combination in NSCs and observed a significant reduction in clonogenic rates, as revealed by neurosphere-forming assay (Figures 8A and B). To understand the role of Trp53inp1 in this context, we transfected specific siTrp53inp1. Trp53inp1 silencing rescued the reduced self-renewal ability of LNA-miR-treated cells that displayed an increased yield of neurosphere formation compared to controls (Figures 8A and B). These observations confirm that Trp53inp1 is responsible for the reduction in NSC self-renewal induced by loss of miR-17/20a. Since high expression of Nanog drives NSCs self-renewal (Po *et al*, 2010), we investigated the role of miR17/20a/Trp53inp1 axis in Nanog activity. Remarkably, siRNA-mediated Trp53inp1 depletion or overexpression of miR17/20a counteracted the reduction in NSC self-renewal observed after siNanog (Figure 8C).
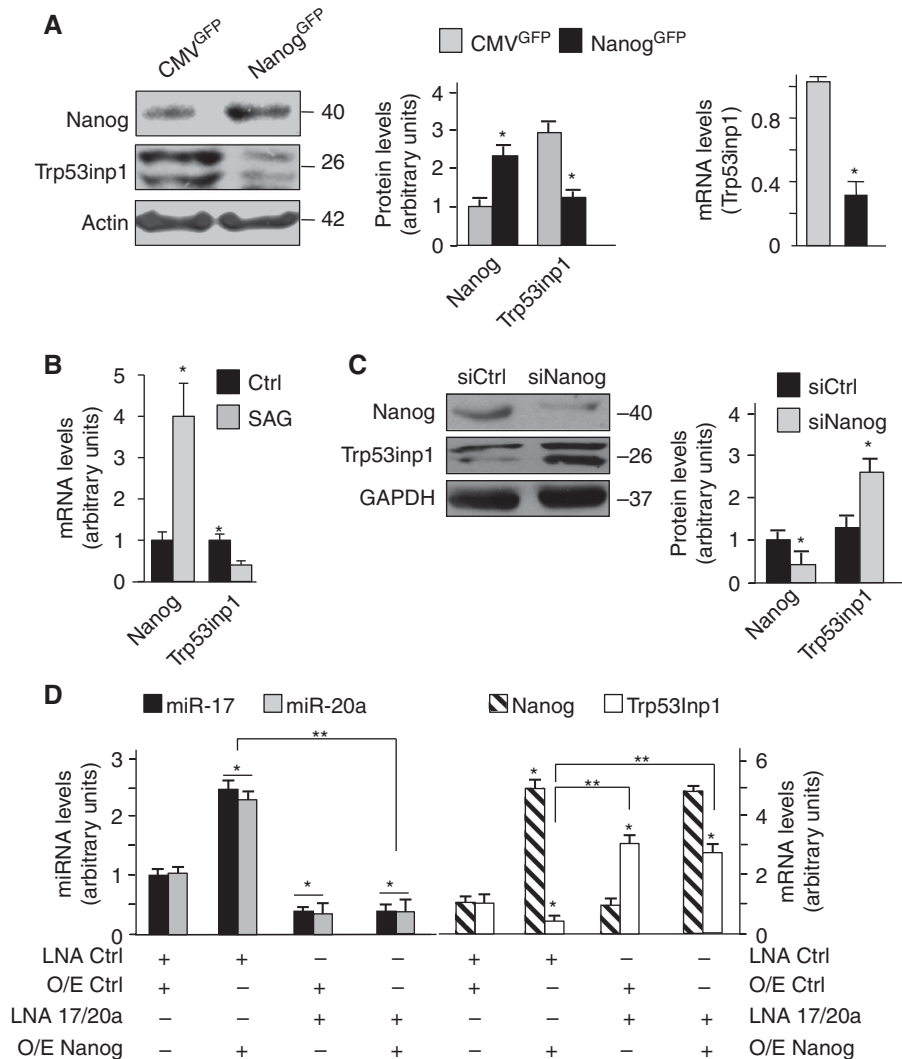
Figure 6 Nanog regulates Trp53inp1 levels. (**A**) Left: western blot analysis (representative image and relative densitometry) of Nanog and Trp53inp1 protein levels in Nanog/GFP-sorted NSCs versus CMV/GFP control cells. Right: Trp53inp1 mRNA levels in the same cellular contexts. Bars represent the mean of three independent experiments ± s.d. *$P < 0.05$ versus Ctrl. (**B**) mRNA levels of Nanog and Trp53inp1 in NSCs untreated and treated with SAG. *, Graph error bars indicate s.d. calculated on at least three independent experiments. $P < 0.05$ versus control (Ctr). (**C**) Western blot analysis (representative image and relative densitometry) of Nanog and Trp53inp1 after siNanog as compared to silencing control (siCtrl) in NSCs. Bars represent the mean of three independent experiments ± s.d $P < 0.05$ versus siCtrl. (**D**) Levels of miR-17 and miR-20a and of Trp53inp1 and Nanog mRNA after LNA-mediated miR-17/20a silencing (LNA 17/20a), overexpression of Nanog (O/E Nanog) and the combination of the two. Graph error bars indicate s.d. calculated on at least three independent experiments. *$P < 0.05$ versus Ctrl, **$P < 0.05$ versus O/E Nanog. Source data for this figure is available on the online supplementary information page.

Overall, our findings indicate that Nanog enhances miR-17/92 cluster expression that in turn targets Trp53inp1, thus contributing to release NSC self-renewal constraints (Figure 8D). These observations suggest that miR-17 and miR-20a are required for Nanog effects on NSC, through inactivation of Trp53inp1.

Discussion

Nanog is known to be critical for the maintenance of ESC (Chambers *et al*, 2003; Mitsui *et al*, 2003) and also recently described to foster self-renewal of postnatal NSCs (Po *et al*, 2010), although the downstream miRNA network has not yet been understood. We describe here the first report of a high-throughput screening of expression profiles of miRNAs regulated by Nanog in postnatal NSCs and identify a number of miRNAs that are modulated following increased or

decreased expression of this transcription factor, suggesting that they might be downstream effectors of Nanog. To gain insights into the transcriptional regulatory networks in ESC cells, ChIP coupled with ultra-high-throughput DNA deep-sequencing (ChIP-seq) has identified the association of the core transcriptional regulatory Oct4/Sox2/Nanog/Tcf3 complex to a number of miRNA promoters (Marson *et al*, 2008). Notably, some of these Oct4/Sox2/Nanog/Tcf3-bound promoters correspond to miRNAs modulated by Nanog in NSCs described in our study (e.g., miR-19b and miR-363), suggesting that they are putative direct targets of this transcription factor and that they are conserved in NSCs. In contrast, the most abundant miR-290/295 cluster in murine ESC, which is also occupied by Oct4/Sox2/Nanog/Tcf3 (Marson *et al*, 2008), is not modulated by Nanog in NSCs, suggesting an miRNA specificity among stem cells lines. Interestingly, a never reported observation of our study is
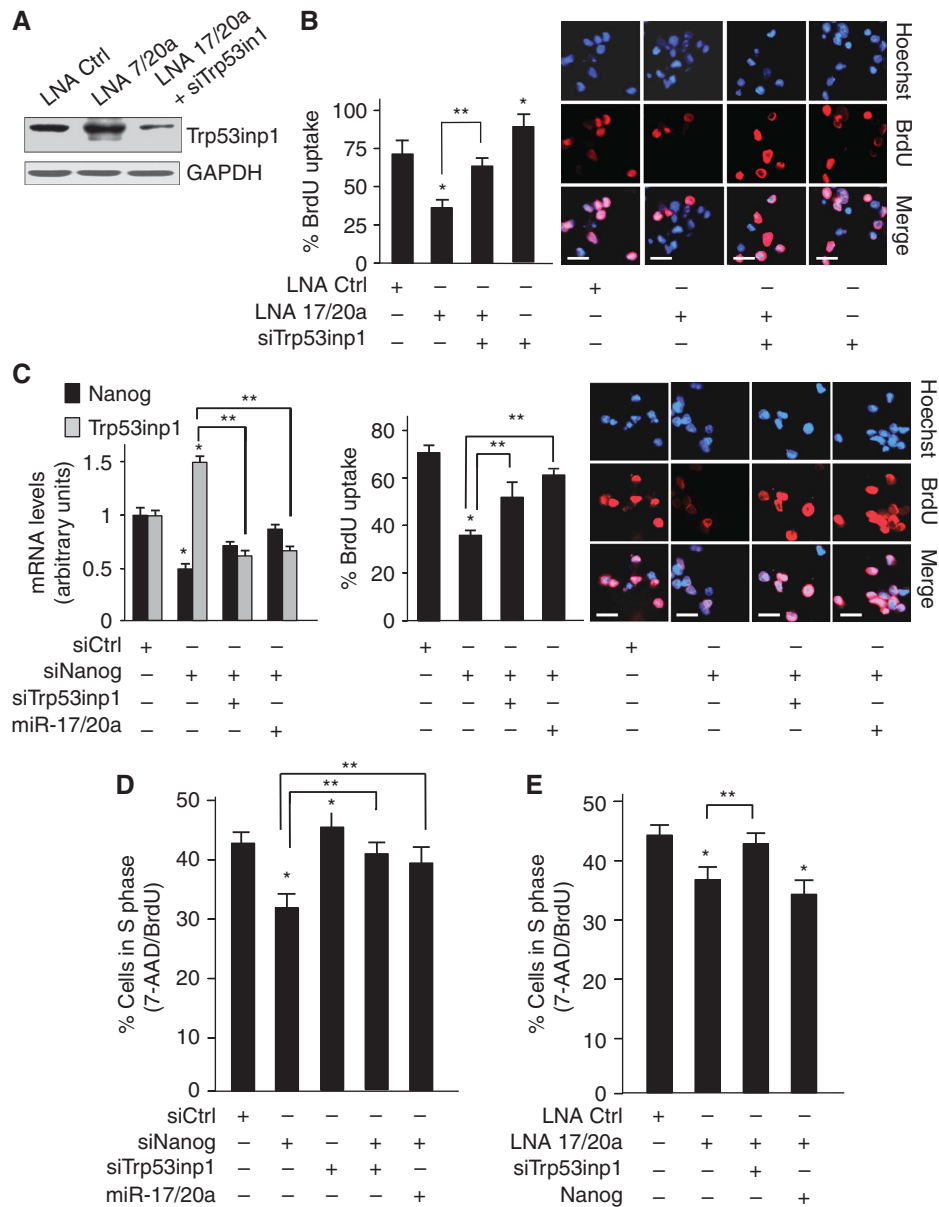
Figure 7 miR-17/20a and Trp53inp1 control NSC proliferation. (**A**) Western blot analysis of endogenous Trp53inp1 protein levels in NSC after LNA anti-miR-17 and -20a without or with siTrp53inp1 compared to scrambled LNA control (LNA-Ctrl). (**B**) BrdU uptake and immunofluorescence images of NSC, LNA-miR-17/20a, or siTrp53inp1 or their combination (Blue: Hoechst, Red: BrdU) (scale bar, 5 µm). Bars represent the mean of three independent experiments ± s.d. *P* < 0.05 versus Ctrl. (**C**) mRNA levels of Nanog and Trp53inp1 and BrdU uptake (with representative images) after siNanog alone or together with siTrp53inp1 or silencing control (siCtrl) and overexpression of miR-17/20a (scale bar, 5 µm). Bars represent the mean of three independent experiments ± s.d. *P* < 0.05 versus siCtrl; **P* < 0.05 versus siNanog. Source data for this figure are available in Supplementary data. (**D**) Histogram shows the percentage of cells in S phase, evaluated by FACS analysis of double staining for BrdU and 7AAD, after siNanog, siTrp53inp1, alone, in combination or together with overexpression of miR-17/20a. Bars represent the mean of three independent experiments ± s.d. *P* < 0.05 versus siCtrl; **P* < 0.05 versus siNanog. (**E**) Histogram shows the percentage of cells in S phase, evaluated by FACS analysis of double staining for BrdU and 7AAD, after LNA anti-miR-17/20a alone or in combination with siTrp53inp1 or Nanog overexpression. Graph error bars indicate s.d. calculated on at least three independent experiments. *P* < 0.05 versus LNA ctrl; **P* < 0.05 versus LNA miR-17/20a. Source data for this figure is available on the online supplementary information page.

the finding of an miR-17/92-Trp53inp1 axis downstream Nanog in NSCs, suggesting a new circuitry involving a Nanog, miRNAs and p53 pathway (Trp53inp1) in neuronal stem cells (Figure 8D).

MiR-17-92 cluster is a novel direct target of Nanog in NSCs

We identify herein that miR-17-92 cluster is a direct transcriptional target of Nanog. This transcription factor binds directly at the miR-17-92 cluster regulatory region and increases the levels of all of the miRNAs belonging to it. This is the first report both of a functional link between Nanog and miR-17-92 cluster and of the ability of miRNA members of the cluster, the miR-17 family, to control NSC features. This strengthened the role of Nanog as a critical player in the homeostatic control of adult neuronal stem cell functions. According to our observations, it has been described that miR-17-92 cluster also controls iPSC, ESC, lung stem cells as
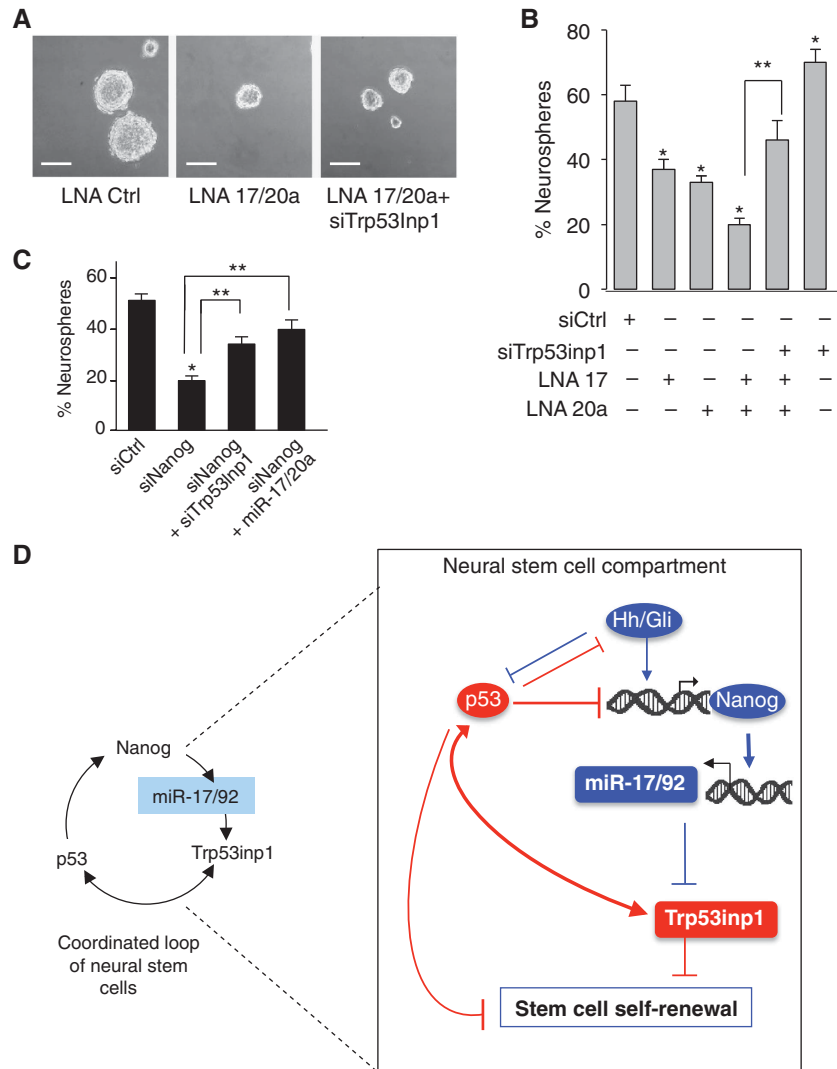
Figure 8 miR-17/20a and Trp53inp1 role in NSC self-renewal. (**A**) Bright-field images of secondary neurosphere-forming assay of NSC transfected with LNA-anti-miR-17/20a alone or in combination with siTrp53inp1 (scale bar, 50 mm). (**B**) Histogram shows the percentage of neurosphere-forming cells after single or combined LNA anti-miR, their combination and the association with siTrp53inp1. Bars represent the mean of three independent experiments ± s.d. *$P < 0.05$ versus siCtrl **$P < 0.05$ versus LNA miR-17/20a. (**C**) Secondary neurosphere-forming assay after silencing of Nanog alone (siNanog) or in combination with siTrp53inp1 or overexpression of miR-17/20a, compared with siCtrl. Graph error bars indicate s.d. calculated on at least three independent experiments. *$P < 0.05$ versus LNA-siCtrl **$P < 0.05$ versus siNanog. (**D**) Model illustrating the coordinated loop among Nanog, p53 and Trp53inp1, centred on miR-17-92 cluster. In NSC, miR-17-92 cluster is regulated by Nanog that is in turn controlled by Hh signalling (Po *et al*, 2010) and p53 (Lin *et al*, 2005). Additional activities of p53 are the direct repression of miR-17/92 cluster (Yan *et al*, 2009) and Hh/Gli (Stecca and Ruiz i Altaba, 2009). In turn, miR-17 and miR-20a, members of miR-17-92 cluster, target and inhibit Trp53inp1 (this study) that inhibits stem cell self-renewal. Red double-arrow line shows the induction of Trp53inp1 by p53 and the backward positive regulation of p53 by Trp53inp1. For further details, see text and references herein.

well as multipotent haematopoietic progenitors (Smith *et al*, 2010; Li *et al*, 2012; Oeztuerk-Winder *et al*, 2012). The ability of Nanog, an Hh target gene, to regulate miR-17-92 cluster highlights the role of developmental signals in the control of miRNAs. Indeed, Hh pathway has been reported to upregulate miR-17-92 cluster through its target MYCN in cerebellar GCPs (Northcott *et al*, 2009; Uziel *et al*, 2009), which are generated upon NSC differentiation *in vitro* and *in vivo* (Klein *et al*, 2005; Po *et al*, 2010). Our study provides a further explanation to the Hh-driven control of miR-17-92 cluster, which is also mediated by the Hh/Gli-induced Nanog expression observed in postnatal cerebellar NSCs (Po *et al*, 2010). We show that Nanog, which is expressed at very high levels in NSCs, as compared to GCPs (Po *et al*, 2010),

enhances miR-17-92 cluster under the control of Hh, thus driving self-renewal. Moreover, these findings boost the knowledge about the Hh/miRNAs interplay. A new axis, including miR-17-92 cluster, controlled by Hh via Nanog, is now added to miRNA/Hh cross-regulation, according to the miRNA-mediated targeting of Smo and Gli1 already reported in GCPs (Ferretti *et al*, 2008).

MiR-17/20a targeting of Trp53inp1 identifies a backward loop in the p53/Nanog network in NSCs

We identify here Trp53inp1 as a novel miR-17/20a target in NSCs. Indeed, Trp53inp1 3′UTR is specifically bound by miR-17 and miR-20a, the two members of miR-17 family, resulting in a decrease in Trp53inp1 protein levels.

Most interestingly, we suggest that miR-17-92 cluster mediates Nanog action upon self-renewal and cell growth. We have described an early burst of Nanog at G1/S transition, with a subsequent increase in miR-17/20a and a decrease in Trp53inp1, suggesting coordination in controlling G1/S transition in NSCs. While these data support the previously described role of Nanog in G1/S transition in human ES cells (Zhang et al, 2009), we suggest that Trp53inp1 contributes Nanog effect on the cell cycle through miR-17/20a in NSC.

The Nanog/miR-17/92/Trp53inp1 axis we have described a novel mechanism that underlies the p53/Nanog network, known to play a crucial role in stem cells. Indeed, Trp53inp1 is involved in cell stress response and is a p53-dependent and -independent inhibitor of cell-cycle progression and promoter of apoptosis (Okamura et al, 2001; Tomasini et al, 2003, 2005). This protein is not only induced by p53, but also controls p53-mediated activity (Okamura et al, 2001; Tomasini et al, 2002). Trp53inp1 co-localizes with p53 and physically interacts with proteins modifying p53 transcriptional activity on several p53 target genes, such as homeodomain-interacting protein kinase-2 (HIPK-2), (Tomasini et al, 2003) that phosphorylates p53 at Ser 46 and enhances its function (D'Orazi et al, 2002).

Trp53inp1 thus appears as a key element in p53-mediated cell-cycle arrest. The oncosuppressor p53 has been described to have a critical function in inhibiting the reprogramming of iPSCs and of pluripotent and self-renewing stem cells and to repress Nanog expression (Lin et al, 2005; Kawamura et al, 2009) as well as NSC proliferation and self-renewal (Meletis et al, 2006). P53 also suppresses Hh pathway (Stecca and Ruiz i Altaba, 2009; Mazzà et al, 2013, in press) that in turn represses p53 (Abe et al, 2008; Stecca and Ruiz i Altaba, 2009). A p53-independent regulation of Nanog and of stemness is also occurring in NSCs, through Gli-mediated direct transcriptional control (Po et al, 2010). Therefore, we speculate that p53 may restrain self-renewing NSC divisions (i) by directly suppressing Nanog expression (Lin et al, 2005); (ii) through cross-inhibition of Hh signalling via Nanog (Po et al, 2010), and (iii) through Trp53inp1 increase, which acts as a suppressor of stem cell self-renewal by acting as a functional positive feedback loop on p53 (i.e., enhancing p21 expression). We speculate that additional Nanog-induced effects might be miR-17/20a-mediated inhibition of p21 (both direct and Trp53inp1-mediated) and Rb1.

In conclusion, we prove that Nanog maintains self-renewal and cell cycle in post-natal NSCs counteracting p53 pathway, at least partially, through miR-17/20a-mediated repression of Trp53inp1.

Materials and methods

Stem cell culture
Mouse cerebella were obtained from postnatal 4-day-old wild-type BL6 mice with the approval of Institutional Review Board (Po et al, 2010). Briefly, tissues were collected in HBSS supplemented with 0.5% glucose and penicillin-streptomycin, grossly triturated with serological pipette and treated with DNAse I to a final concentration of 0.04% for 20 min. Finally, cell aggregates were mechanically dissociated using pipettes of decreasing bore size to obtain a single-cell suspension. Cells were cultured as neurospheres in selective medium after centrifugation; DMEM/F12 supplemented with 0.6% glucose, 25 mg/ml insulin, 60 mg/ml N-acetyl-L-cysteine, 2 mg/ml heparin, 20 ng/ml EGF, 20 ng/ml bFGF (Peprotech, Rocky Hill, NJ),

$1 \times$ penicillin-streptomycin and B27 supplement without vitamin A. For the neurosphere-forming assay, cells were plated at clonal density $(1–2 \text{ cells/mm}^2)$ into 96-well plates and cultured in selective medium as described above. For differentiation studies, neurospheres were mechanically dissociated, and the resulting cells were plated onto D-poly-Lysine-coated dishes in differentiation medium (DMEM/F12 with N2 supplement and 2 mg/ml heparin, 0.6% glucose, 60 mg/ml N-acetyl-L-cysteine, containing 1% Calf Serum and PDGF 10 ng/ml (Sigma, P3076) or RA 2 μM (Sigma, R2625), for 4 days. Unless otherwise indicated, media and supplements for cell culture were purchased from Gibco-Invitrogen (Carlsbad, CA) and chemicals were purchased from Sigma-Aldrich (St Louis, MO). Neurospheres were transduced with pGreenZeo Lentiviral Reporter Vectors containing specific promoters for NANOG (Nanog-GFP) or CMV (CMV-GFP) (Biocat, Heidelberg, Germany). For overexpression studies, Nanog vector (pPYCAG-IP-Nanog-IRES-EGFP) and control plasmid (pPYCAG-IP-IRES-EGFP) were kindly provided by Dr Fiona Watt, University of Cambridge, UK. NSC images were acquired using the EVOS xl core digital inverted microscope (AMG). Neurospheres were treated with Smo-agonist SAG (200 nM, Alexis).

For cell-cycle analysis, Nocodazole (Sigma-Aldrich) was added at the concentration of 500 ng/ml for 12 h for synchronization in G2 phase, cells were then washed to remove Nocodazole and put in stem medium to allow cell-cycle progression. Cells were then stopped at given points for FACS, RNA, and protein analyses and for immunofluorescence investigations. All experiments were performed at least in triplicate and results represented as mean values ± s.d.

Fluorescence-activated cell sorting
Mechanically dissociated cells transduced with Nanog-GFP or with CMV-GFP were sorted by fluorescence-activated cell sorting, FACS Aria (Becton Dickinson, NJ).

Mechanically dissociated fresh mouse cerebella cells were stained with anti-Prominin1-PE (Miltenyi Biotec) according to the manufacturing instructions and sorted by FACS Aria.

For visualization of cells in different phases of cell cycle, cells were fixed with 70% ethanol for 2 h at +4°C; cells were then washed and incubated overnight with 25 μg/ml 7-AAD (Sigma) and 40 mg/ml RNAse A (Sigma) in PBS.

For double staining, first cells were pulsed for 3 h with BrdU, then were fixed in 30% Methanol and 0.4% PFA and incubated for 15 min with 500 000 U/ml DNAse (Sigma). Fixed cells were washed and incubated with Anti-BrdU–APC (BD Pharmingen) for 1 h at RT. Finally, cells were counterstained with 7-AAD.

For endogenous Nanog visualization by FACS, antibody Alexa Fluor 647 Mouse anti-mouse Nanog (560279; BD Pharmingen) and Alexa Fluor 647 Mouse IgG1K Isotype Control (557732; BD Pharmingen) were used. In both cases, cells were counterstained with 7-AAD. The staining procedure was done according to the manufacturer's instructions (Catalogue Number: 00-5523, eBioscience, CA). Briefly, two million cells were fixed with 1 ml Fixation/Permeabilization solution, pulse vortexed and incubated at 4°C or at room temperature for 60 min in the dark. Fixed cells were then permeabilized, stained using Nanog Alexa-Flour or Isotype control and visualized by FACS on FACSCalibur using the CellQuest software (both from BD Biosciences, San Jose, CA, USA).

RNA isolation and real-time qPCR
RNA isolation from cells and tissue samples was performed as described previously (Ferretti et al, 2006). cDNA synthesis was performed using the High Capacity cDNA reverse transcription kit from Applied Biosystems (Foster City, CA). Quantitative reverse transcription (RT–PCR) analysis of Nanog, Gli1, βIII-tubulin, CcnD1, Smo, Trp53inp1, β-actin, β2 microglobulin, and Hprt mRNA expression was performed on cDNAs employing the ABI Prism 7900HT Sequence Detection System (Applied Biosystems) using TaqMan gene expression assay according to the manufacturer's instructions (Applied Biosystems/LifeTech). Each amplification reaction was performed in triplicate, and the average of the three threshold cycles was used to calculate the amount of transcripts in the sample (SDS software, AB). mRNA quantification was expressed, in arbitrary units, as the ratio of the sample quantity to the calibrator or to the mean values of control samples. All values were normalized to three endogenous controls, β-actin, β2

microglobulin and Hprt. MiRNA expression using Taqman probe was performed as described earlier (Ferretti *et al*, 2008) using the following miRNAs: miR-17-5p (Code:002308), miR-18a-5p (Code: 002422), miR-19-3p (Code:000395), miR-19b-3p (Code:000396), miR-20a-5p (Code:000580), miR-20b-5p (Code:001014), and miR-92a-3p (Code:000430).

Western blot assay

Cells were lysed in Tris–HCl pH 7.6, 50 mM, deoxycholic acid sodium salt 0.5%, NaCl 140 mM, NP-40 1%, EDTA 5 mM, NaF 100 mM, Na pyrophosphate 2 mM and protease inhibitors. Lysates were separated on 8 or 10% acrylamide or pre-cast gel (4–12%, Invitrogen) and immunoblotted using standard procedures. Anti-Mouse Nanog (RCAB0001P; Cosmo Bio Co, Japan), anti-Gli1 H-300 (sc-20687; Santa Cruz Biotechnology, CA), anti-Prominin1 (Ab16518-Abcam, MA), anti-Smo N-19 (sc-6366; Santa Cruz Biotechnology), anti-mouse βIII-Tubulin (MAB 1637; Millipore), anti-Trp53inp1 (sc-68919; Santa Cruz Biotechnology), anti-CyclinD1 (sc-246; Santa Cruz Biotechnology), anti-p21 (sc-397; Santa Cruz Biotechnology), anti-GAPDH (ab8245; Abcam, MA), anti-Actin I19 (sc-1616; Santa Cruz Biotechnology) and HRP-conjugated secondary antisera (Santa Cruz Biotechnology) were used followed by enhanced chemiluminescence (ECL Amersham, Amersham, UK).

Densitometry calculations for western blot were calculated using the ImageJ software, verifying for non-saturation and subtracting background. Values are expressed as the integrals of each band normalized to weakest band.

miRNA expression profiling

Analysis of the expression profiling of 550 mouse miRNAs was carried out on RNA samples according to Applied Biosystems protocols, as described previously (Ferretti *et al*, 2009). The assay included RT with specific stem-loop primers followed by real-time qPCR using miRNA-specific TaqMan MGB probe and TaqMan universal master mix in an Applied Biosystems 7900HT PCR system. Pre-processing of raw data files consisted of threshold and baseline corrections for each sample, with each amplification plot assessed to confirm that the threshold cycle (Ct) value corresponded with the midpoint of logarithmic amplification (SDS 2.3, Life Technologies). For all miRNA quantification experiments, cycle threshold (Ct) values greater than 36 were excluded. Values were normalized against the expression levels of RNU6B and RNU48 and Delta Ct values were calculated using the Real-Time StatMiner software (Integromics TM, Philadelphia, PA). The same software was used to generate unsupervised hierarchical clustering based on the support tree average linkage with and Euclidean correlations.

Overexpression and knockdown studies

Synthetic miRIDIAN mimic (miR-17, code: C-310561-07-0010; miR-20a, code: C-310514-05-0010) or negative control (miRIDIAN mimic negative control, code: CN-0010000-01-05) (Dharmacon) was transfected into cells using the DharmaFECT Duo transfection reagent (Dharmacon) at 100 nM. SiGlo Green and siGLO Red transfection control reagents (10 nM) (Dharmacon) were used to verify transfection efficiency that ranged between 75 and 85%. Antagomir-mediated miRNA knockdown was carried out using fluorescein-labelled LNA oligonucleotides (Exiqon, Vedbaek, Denmark; miR-17: code 426848-00, miR-20a: code 411929-08) or combination of these miRNAs and scrambled control (Exiqon mirCURY knockdown probe control A: code 199002-08) (Exiqon), transfected into NSC cells at a final concentration of 50 nM by Hiperfect reagent (Qiagen, Hilden, Germany). Transfection efficiency ranged between 70 and 80%. siRNA for mouse Nanog (siNanog) and control (code AM4611) were obtained from Ambion-Applied Biosystems protocols. For Trp53inp1 silencing, a pool of three pre-designed siRNAs from Ambion-Life Technologies was used (ID: s82034, s82035, and s82036,) and silencing control was negative control 2 siRNA (code: 4390847). Transfection of siRNA duplexes (40 nM) was carried out using the Hiperfect reagent (Qiagen) according to the manufacturer's instructions. Transfections were carried out for 48 h.

Chromatin immunoprecipitation

ChIP was performed as described earlier (Canettieri *et al*, 2010). Briefly, cells were cross-linked 10 min with 1% formaldehyde, and the reaction was stopped with 0.125 M glycine for 5 min. Cells were washed and harvested, and cytoplasmic membranes were lysed with lysis buffer (5 mM Pipes, 85 mM KCl, and 0.5% Nonidet P-40). After centrifugation, nuclei were lysed with sonication buffer (in 1% SDS, 10 mM EDTA, and 50 mM Tris (pH 8) supplemented with protease inhibitors) to obtain chromatin fragments of about 400–600 nucleotides. After sonication, lysates were precleared for 1 h, diluted with nine volumes of dilution buffer (0.01% SDS, 1.2 mM EDTA, 16.7 mM Tris–HCl (pH 8), 1.1% Triton X-100 and 167 mM NaCl) and incubated with the specific antibodies overnight. The next day, salmon sperm-saturated protein A beads (Upstate) were added for 40 min, after which the lysates were washed five times with Buffer A (0.1% SDS, 2 mM EDTA, 20 mM Tris–HCl (pH 8), 1% Triton X-100 and 150 mM NaCl), four times with Buffer B (0.1% SDS, 2 mM EDTA, 20 mM Tris–HCl (pH 8), 1% Triton X-100 and 500 mM NaCl), and once with Buffer TE (10 mM Tris–HCl (pH 8) and 1 mM EDTA). After the final washing, the immunecomplexes were eluted with elution buffer (1% SDS and 100 mM NaHCO$_3$) for 30 min at room temperature and, after the addition of 200 mM NaCl, the cross-linking was reversed with an overnight incubation at 65°C. Subsequently, samples were digested with proteinase K and RNase A for 2 h at 42°C, and the DNA was purified and precipitated. The following antibodies were used: rabbit monoclonal anti-Nanog (Cell Signaling, code: 8600), rabbit polyclonal anti-acetyl-histone 3 (Millipore, code: 06599), normal rabbit IgG (sc-2027). Eluted DNA was analysed with standard PCR techniques or real-time qPCR. Primers were designed with the Primer Design and Search Tool. The reaction was carried out using the following primers:

Primers for miR 17-92 upstream region (RT–qPCR):
Site miR 17-92 s1 Fw: TTGTAGGACCCTTATTGTGTGTTTTT
Site miR 17-92 s1 Rev: CAAATTGGACACATGTAAGCCTTAA
Site miR 17-92 s2 Fw: GGATAGAATTGCCCCTTAGGAAGA
Site miR 17-92 s2 Rev: AGGGTAAGCACATTTGCTCAAAA
Site miR 17-92 s3 Fw: TTGCTGCTACTCATCTTGCAGTATT
Site miR 17-92 s3 Rev: AGTTGAAAAACCCACCAAGATTCA
Primers for miR 17/92 upstream region (PCR):
Site s1 Fw: CCTGGTCAATGTGAGGCTTT
Site s1 Rev: GCCAAAGCTCTAAATTCTGT
Site s2 Fw: GGATGTGAATCTTGGTGGGT
Site s2 Rev: ACGTGTATGACTAGGGTTGG
Site s3 Fw: CCTGGTTGCCCTTTTTCTCT
Site s3 Rev: CCCATTCCAAGTTGCTCTTC
Primers for miR-106b-25 upstream region (RT–qPCR)
Site miR-106b-25 s1 Fw: CACCTCACCTAATGACCCTCAAG
Site miR-106b-25 s1 Rev: CGGTAGCACAGAGAGGACCACTA
Site miR-106b-25 s2 Fw: CACATGGTCTCTGAAGTCTGTCAAG
Site miR-106b-25 s2 Rev: AACTTCCAACTTTTCAGGAGAATGA
Site miR-106b-25 s3 Fw: GATTCTCACCACGCTCAATGC
Site miR-106b-25 s3 Rev: GCCGGAAGCTGGACGTT
Site miR-106b-25 s4 Fw: AGAGTTGAGGACAGAGGCCATTA
Site miR-106b-25 s4 Rev: GGGTGCCATCTTGCAGGTT
Primers for beta-actin (PCR and RT–qPCR)
Fw: AGAGGGAAATCGTGCGTGAC
Rev: AACCGCTCGTTGCCAATAGT

Luciferase assays

Mouse miR-17-92 promoter_luciferase vector (−1273 bp) was obtained from Genecoepia (Catalogue No. CS-MmiPRM3357-PG04, Gene Accession: MI0000567). Mouse Nanog promoter_luciferase vector (−2500 bp) (Nanog5P reporter) was obtained from Addgene (code: Plasmid 16337, Cambridge, MA). NSCs were transfected in 24-well plates with 80 ng of Nanog or miR-17/92 promoter_luciferase vector, 400 ng of Nanog or mock and 5 ng of or pRL-CMV-Renilla Luciferase control vector with the Fugene6 Transfection Reagent (Roche, Basel, Switzerland). Cells were harvested and tested 24 h post transfection with the dual-luciferase assay (Promega). Empty pGL4 vector was tested as a negative control with Nanog or mock. Results are expressed as luciferase/renilla ratios and represent the average ± s.d. of at least three experiments, each performed in triplicate.

miRNA target sites in 3′UTR Trp53inp1 gene regions were identified by bioinformatic analysis using the following online databases: Target Scan (http://www.targetscan.org), pictar (http://pictar.mdc-berlin.de/), and MiRBase Sanger (http://microrna.sanger.ac.uk/cgi-bin/targets/v5/search.pl) (only those putative miRNA target sites resulting from at least two databases were considered as positive). The entire 3′UTR region (4418 bp) of Trp53inp1 was cloned by

Genecopoeia and divided into two regions: UTR length 1–2275 bp (Catalogue No. MmiT032758a-MT05, Gene Accession: NM_021897.3) and 2131–4418 bp (Catalogue No. MmiT032758b-MT05, Gene Accession: NM_021897.3). These constructs were used to generate, by site-directed mutagenesis as described later, the mutant derivatives lacking miRNA-binding sites. NSCs were cultured in 24-well plates and transfected first with 100 nM of synthetic miRNA (17, 20a) or scramble control and after 24 h with 0.1 mg of specific 3′UTR or 0.3 mg of negative control vector (Genecopoeia, Catalogue No. CmiT000001.MT05). Cells were harvested and tested 24 h post second transfection with the dual-luciferase assay (Promega). All luciferase activity data are presented as means ± s.d. of values from at least three experiments, each performed in triplicate.

Site-directed mutagenesis

Mutation by deletion of critical nucleotides in Nanog-binding sites was designed according to Pavletich and Pabo (1993) and Mizugishi *et al* (2001). To mutagenize the promoter constructs, the QuickChange Lightening Site-Directed Mutagenesis Kit (Agilent) was used. The reaction was carried out according to the manufacturers' protocol using the following primers:

s1 miR-17/92 NBS Fw: GGGGAAGCCTACTGTAAAAGCCAAGGGATTGTATCTTA

s1 miR-17/92 NBS Rev: TAAGATACAATCCCTTGGCTTTTACAGTAGGCTTCCCC

s2 miR-17/92 NBS Fw: TAGGAAGATTAAGAGAAGAGCAACTGCTCGGAAAGTGG

s2 miR-17/92 NBS Rev: CCACTTTCCGAGCAGTTGCTCTTCTCTTAATCTTCCTA

s3 miR-17/92 NBS Fw: TACTCATCTTGCAGTATTTCGCACGGATGTGAATCTTGG

s3 miR-17/92 NBS Rev: CCAAGATTCACATCCGTGCGAAATACTGCAAGATGAGTA

Mutation by deletion of critical in miRNA-binding sites in Trp53inp1 site was designed as mentioned above. The reaction was carried out using the following primers:

s1 Trp53inp1 3′UTR Fw: GATGGGTTGGTTTCCACAAG

s1 Trp53inp1 3′UTR Rev: CCTGCTGTGGTAAGTATTAGT

s2 Trp53inp1 3′UTR Fw: GGTCAGAGATGGTCAGTTTT

s2 Trp53inp1 3′UTR Rev: GAACCCATTACAAAGAACTG

Cell proliferation assay

Cell proliferation of NSCs was evaluated by BrdU incorporation (24 h pulse). Cells were plated on poly-lysine-coated Lab-Tek chamber slides (coverslips) and allowed to adhere for 3 h and then fixed with 4% paraformaldehyde, permeabilized with 0.1% Triton X-100, and BrdU detection (Roche) was performed according to the manufacturer's instructions. 594-conjugated anti-mouse secondary antibody was purchased from Molecular Probes (Invitrogen, Eugene, OR). Nuclei were counterstained with the Hoechst reagent.

Coverslips were mounted with fluorescence mounting medium (S3023) (Dako, Carpinteria, CA). Images were taken with a digital camera (ProgRes C10 plus, Zeiss) interfaced to a computer with IAS 2000 software version 009000 (Delta Sistemi, Rome, Italy) using the Leica DM2500 microscope. At least 300 nuclei were counted in triplicate, and the number of BrdU-positive nuclei was recorded. Results are represented as mean values ± s.d. from at least three biological replicas.

Statistical analysis

For all miRNA analysis experiments, Wilcoxon signed-rank test was used using the StatMiner software (Integromics, TM) to generate Delta-Delta Ct values for each comparison. *P*-values were adjusted using the FDR Benjamini-Hochberg method, and significance was attributed with FDR < 0.05 for all analyses. Supervised hierarchical clustering of differentially expressed miRNAs in HN-NSC versus LN-NSC was generated by the Permutmatrix software according to Delta Ct values. The clustering and tree are based on the Euclidean correlation, complete linkage, and Unidimensional scaling. Statistical analysis of biological experimental triplicates was performed using the StatView 4.1 software (Abacus Concepts, Berkeley, CA). Statistical differences were analysed by Mann–Whitney *U* test for non-parametric values. The results are expressed as mean ± s.d. from an appropriate number of experiments as indicated in the figure legends.

Supplementary data

Supplementary data are available at *The EMBO Journal* Online (http://www.embojournal.org).

Conflict of interest

The authors declare that they have no conflict of interest.

References

Abe Y, Oda-Sato E, Tobiume K, Kawauchi K, Taya Y, Okamoto K, Oren M, Tanaka N (2008) Hedgehog signaling overrides p53-mediated tumor suppression by activating Mdm2. *Proc Natl Acad Sci USA* **105:** 4838–4843

Blakaj A, Lin H (2008) Piecing together the mosaic of early mammalian development through microRNAs. *J Biol Chem* **283:** 9505–9508

Brambrink T, Foreman R, Welstead GG, Lengner CJ, Wernig M, Suh H, Jaenisch R (2008) Sequential expression of pluripotency markers during direct reprogramming of mouse somatic cells. *Cell Stem Cell* **2:** 151–159

Brett JO, Renault VM, Rafalski VA, Webb AE, Brunet A (2011) The microRNA cluster miR-106b∼25 regulates adult neural stem/progenitor cell proliferation and neuronal differentiation. *Aging* **3:** 108–124

Canettieri G, Di Marcotullio L, Greco A, Coni S, Antonucci L, Infante P, Pietrosanti L, De Smaele E, Ferretti E, Miele E, Pelloni M, De Simone G, Pedone EM, Gallinari P, Giorgi A, Steinkuhler C, Vitagliano L, Pedone C, Schinin ME, Screpanti I *et al* (2010) Histone deacetylase and Cullin3-REN(KCTD11)

ubiquitin ligase interplay regulates Hedgehog signalling through Gli acetylation. *Nat Cell Biol* **12:** 132–142

Chambers I, Colby D, Robertson M, Nichols J, Lee S, Tweedie S, Smith A (2003) Functional expression cloning of Nanog, a pluripotency sustaining factor in embryonic stem cells. *Cell* **113:** 643–655

Chen X, Fang F, Liou YC, Ng HH (2008a) Zfp143 regulates Nanog through modulation of Oct4 binding. *Stem Cells* **26:** 2759–2767

Chen X, Xu H, Yuan P, Fang F, Huss M, Vega VB, Wong E, Orlov YL, Zhang W, Jiang J, Loh YH, Yeo HC, Yeo ZX, Narang V, Govindarajan KR, Leong B, Shahab A, Ruan Y, Bourque G, Sung WK *et al* (2008b) Integration of external signaling pathways with the core transcriptional network in embryonic stem cells. *Cell* **133:** 1106–1117

D'Orazi G, Cecchinelli B, Bruno T, Manni I, Higashimoto Y, Saito S, Gostissa M, Coen S, Marchetti A, Del Sal G, Piaggio G, Fanciulli M, Appella E, Soddu S (2002) Homeodomain-interacting protein kinase-2 phosphorylates p53 at Ser 46 and mediates apoptosis. *Nat Cell Biol* **4:** 11–19

Ferretti E, De Smaele E, Po A, Di Marcotullio L, Tosi E, Espinola MS, Di Rocco C, Riccardi R, Giangaspero F, Farcomeni A, Nofroni I,

Laneve P, Gioia U, Caffarelli E, Bozzoni I, Screpanti I, Gulino A (2009) MicroRNA profiling in human medulloblastoma. *Int J Cancer* **124:** 568–577

Ferretti E, De Smaele E, Miele E, Laneve P, Po A, Pelloni M, Paganelli A, Di Marcotullio L, Caffarelli E, Screpanti I, Bozzoni I, Gulino A (2008) Concerted microRNA control of Hedgehog signalling in cerebellar neuronal progenitor and tumour cells. *EMBO J* **27:** 2616–2627

Ferretti E, Di Marcotullio L, Gessi M, Mattei T, Greco A, Po A, De Smaele E, Giangaspero F, Riccardi R, Di Rocco C, Pazzaglia S, Maroder M, Alimandi M, Screpanti I, Gulino A (2006) Alternative splicing of the ErbB-4 cytoplasmic domain and its regulation by hedgehog signaling identify distinct medulloblastoma subsets. *Oncogene* **25:** 7267–7273

Kawamura T, Suzuki J, Wang YV, Menendez S, Morera LB, Raya A, Wahl GM, Izpisua Belmonte JC (2009) Linking the p53 tumour suppressor pathway to somatic cell reprogramming. *Nature* **460:** 1140–1144

Kim YK, Kim VN (2007) Processing of intronic microRNAs. *EMBO J* **26:** 775–783

Klein C, Butt SJ, Machold RP, Johnson JE, Fishell G (2005) Cerebellum- and forebrain-derived stem cells possess intrinsic regional character. *Development* **132:** 4497–4508

Lee A, Kessler JD, Read TA, Kaiser C, Corbeil D, Huttner WB, Johnson JE, Wechsler-Reya RJ (2005) Isolation of neural stem cells from the postnatal cerebellum. *Nat Neurosci* **8:** 723–729

Lewitzky M, Yamanaka S (2007) Reprogramming somatic cells towards pluripotency by defined factors. *Curr Opin Biotechnol* **18:** 467–473

Li Y, Vecchiarelli-Federico LM, Li YJ, Egan SE, Spaner D, Hough MR, Ben-David Y (2012) The miR-17-92 cluster expands multipotent hematopoietic progenitors whereas imbalanced expression of its individual oncogenic miRNAs promotes leukemia in mice. *Blood* **119:** 4486–4498

Li Z, Yang CS, Nakashima K, Rana TM (2011) Small RNA-mediated regulation of iPS cell generation. *EMBO J* **30:** 823–834

Lin T, Chao C, Saito S, Mazur SJ, Murphy ME, Appella E, Xu Y (2005) p53 induces differentiation of mouse embryonic stem cells by suppressing Nanog expression. *Nat Cell Biol* **7:** 165–171

Marson A, Levine SS, Cole MF, Frampton GM, Brambrink T, Johnstone S, Guenther MG, Johnston WK, Wernig M, Newman J, Calabrese JM, Dennis LM, Volkert TL, Gupta S, Love J, Hannett N, Sharp PA, Bartel DP, Jaenisch R, Young RA (2008) Connecting microRNA genes to the core transcriptional regulatory circuitry of embryonic stem cells. *Cell* **134:** 521–533

Mazzà D, Infante P, Colicchia V, Greco A, Alfonsi R, Siler M, Antonucci L, Po A, Capalbo C, De Smaele E, Ferretti E, Canettieri G, Giannini G, Screpanti I, Gulino A, Di Marcotullio L (2013) PCAF ubiquitin ligase activity inhibits Hedgehog/Gli1 signaling in p53-dependent response to genotoxic stress. *Cell Death Diff* in press

Meletis K, Wirta V, Hede SM, Nister M, Lundeberg J, Frisen J (2006) p53 suppresses the self-renewal of adult neural stem cells. *Development* **133:** 363–369

Mitsui K, Tokuzawa Y, Itoh H, Segawa K, Murakami M, Takahashi K, Maruyama M, Maeda M, Yamanaka S (2003) The homeoprotein Nanog is required for maintenance of pluripotency in mouse epiblast and ES cells. *Cell* **113:** 631–642

Mizugishi K, Aruga J, Nakata K, Mikoshiba K (2001) Molecular properties of Zic proteins as transcriptional regulators and their relationship to GLI proteins. *J Biol Chem* **276:** 2180–2188

Northcott PA, Fernandez LA, Hagan JP, Ellison DW, Grajkowska W, Gillespie Y, Grundy R, Van Meter T, Rutka JT, Croce CM, Kenney AM, Taylor MD (2009) The miR-17/92 polycistron is up-regulated in sonic hedgehog-driven medulloblastomas and induced by N-myc in sonic hedgehog-treated cerebellar neural precursors. *Cancer Res* **69:** 3249–3255

Oeztuerk-Winder F, Guinot A, Ochalek A, Ventura JJ (2012) Regulation of human lung alveolar multipotent cells by a novel p38alpha MAPK/miR-17-92 axis. *EMBO J* **31:** 3431–3441

Okamura S, Arakawa H, Tanaka T, Nakanishi H, Ng CC, Taya Y, Monden M, Nakamura Y (2001) p53DINP1, a p53-inducible gene, regulates p53-dependent apoptosis. *Mol Cell* **8:** 85–94

Pan G, Thomson JA (2007) Nanog and transcriptional networks in embryonic stem cell pluripotency. *Cell Res* **17:** 42–49

Pavletich NP, Pabo CO (1993) Crystal structure of a five-finger GLI-DNA complex: new perspectives on zinc fingers. *Science* **261:** 1701–1707

Po A, Ferretti E, Miele E, De Smaele E, Paganelli A, Canettieri G, Coni S, Di Marcotullio L, Biffoni M, Massimi L, Di Rocco C, Screpanti I, Gulino A (2010) Hedgehog controls neural stem cells through p53-independent regulation of Nanog. *EMBO J* **29:** 2646–2658

Silva J, Nichols J, Theunissen TW, Guo G, van Oosten AL, Barrandon O, Wray J, Yamanaka S, Chambers I, Smith A (2009) Nanog is the gateway to the pluripotent ground state. *Cell* **138:** 722–737

Smith KN, Singh AM, Dalton S (2010) Myc represses primitive endoderm differentiation in pluripotent stem cells. *Cell Stem Cell* **7:** 343–354

Stecca B, Ruiz i Altaba A (2009) A GLI1-p53 inhibitory loop controls neural stem cell and tumour cell numbers. *EMBO J* **28:** 663–676

Stefani G, Slack FJ (2008) Small non-coding RNAs in animal development. *Nat Rev Mol Cell Biol* **9:** 219–230

Takahashi K, Yamanaka S (2006) Induction of pluripotent stem cells from mouse embryonic and adult fibroblast cultures by defined factors. *Cell* **126:** 663–676

Tay Y, Zhang J, Thomson AM, Lim B, Rigoutsos I (2008a) MicroRNAs to Nanog, Oct4 and Sox2 coding regions modulate embryonic stem cell differentiation. *Nature* **455:** 1124–1128

Tay YM, Tam WL, Ang YS, Gaughwin PM, Yang H, Wang W, Liu R, George J, Ng HH, Perera RJ, Lufkin T, Rigoutsos I, Thomson AM, Lim B (2008b) MicroRNA-134 modulates the differentiation of mouse embryonic stem cells, where it causes post-transcriptional attenuation of Nanog and LRH1. *Stem Cells* **26:** 17–29

Tomasini R, Seux M, Nowak J, Bontemps C, Carrier A, Dagorn JC, Pébusque MJ, Iovanna JL, Dusetti NJ (2005) TP53INP1 is a novel p73 target gene that induces cell cycle arrest and cell death by modulating p73 transcriptional activity. *Oncogene* **24:** 8093–8104

Tomasini R, Samir AA, Carrier A, Isnardon D, Cecchinelli B, Soddu S, Malissen B, Dagorn JC, Iovanna JL, Dusetti NJ (2003) TP53INP1s and homeodomain-interacting protein kinase-2 (HIPK2) are partners in regulating p53 activity. *J Biol Chem* **278:** 37722–37729

Tomasini R, Samir AA, Pebusque MJ, Calvo EL, Totaro S, Dagorn JC, Dusetti NJ, Iovanna JL (2002) P53-dependent expression of the stress-induced protein (SIP). *Eur J Cell Biol* **81:** 294–301

Tomasini R, Samir AA, Vaccaro MI, Pebusque MJ, Dagorn JC, Iovanna JL, Dusetti NJ (2001) Molecular and functional characterization of the stress-induced protein (SIP) gene and its two transcripts generated by alternative splicing. SIP induced by stress and promotes cell death. *J Biol Chem* **276:** 44185–44192

Uziel T, Karginov FV, Xie S, Parker JS, Wang YD, Gajjar A, He L, Ellison D, Gilbertson RJ, Hannon G, Roussel MF (2009) The miR-17~92 cluster collaborates with the Sonic Hedgehog pathway in medulloblastoma. *Proc Natl Acad Sci USA* **106:** 2812–2817

Vidigal JA, Ventura A (2012) Embryonic stem cell miRNAs and their roles in development and disease. *Semin Cancer Biol* **22:** 428–436

Wu Q, Chen X, Zhang J, Loh YH, Low TY, Zhang W, Sze SK, Lim B, Ng HH (2006) Sall4 interacts with Nanog and co-occupies Nanog genomic sites in embryonic stem cells. *J Biol Chem* **281:** 24090–24094

Yan HL, Xue G, Mei Q, Wang YZ, Ding FX, Liu MF, Lu MH, Tang Y, Yu HY, Sun SH (2009) Repression of the miR-17-92 cluster by p53 has an important function in hypoxia-induced apoptosis. *EMBO J* **28:** 2719–2732

Zbinden M, Duquet A, Lorente-Trigos A, Ngwabyt SN, Borges I, Ruiz i Altaba A (2010) NANOG regulates glioma stem cells and is essential *in vivo* acting in a cross-functional network with GLI1 and p53. *EMBO J* **29:** 2659–2674

Zhang X, Neganova I, Przyborski S, Yang C, Cooke M, Atkinson SP, Anyfantis G, Fenyk S, Keith WN, Hoare SF, Hughes O, Strachan T, Stojkovic M, Hinds PW, Armstrong L, Lako M (2009) A role for NANOG in G1 to S transition in human embryonic stem cells through direct binding of CDK6 and CDC25A. *J Cell Biol* **184:** 67–82